Insight into reactions and interface between boron nitride nanotube and aluminum

Debrupa Lahiri
Department of Mechanical and Materials Engineering, Plasma Forming Lab, Florida International University, Miami, Florida 33174

Virendra Singh
AMPAC and Nanoscience Technology Center, University of Central Florida, Orlando, Florida 32816

Lu Hua Li and Tan Xing
ARC Centre of Excellence for Functional Nanomaterials, Institute for Technology Research and Innovation, Deakin University, Waurn Ponds, Victoria 3216, Australia

Sudipta Seal
AMPAC and Nanoscience Technology Center, University of Central Florida, Orlando, Florida 32816

Ying Chen
ARC Centre of Excellence for Functional Nanomaterials, Institute for Technology Research and Innovation, Deakin University, Waurn Ponds, VIC 3216, Australia

Arvind Agarwal[a)]
Department of Mechanical and Materials Engineering, Plasma Forming Lab, Florida International University, Miami, Florida 33174

(Received 13 April 2012; accepted 7 August 2012)

Nature and mechanism of interfacial reactions between boron nitride nanotubes (BNNTs) and aluminum matrix at high temperature (650 °C) are studied using high-resolution transmission electron microscopy (HRTEM). This study analyzes the feasibility of the use of BNNTs as reinforcement in aluminum matrix composites for structural application, for which interface plays a critical role. Thermodynamic comparison of aluminum (Al)-BNNT with analogous Al-carbon nanotube (Al-CNT) system reveals lesser amount of reaction in the former. Experimental observation also reveals thin (~7 nm) reaction-product formation at Al-BNNT interface even after 120 min of exposure at 650 °C. The spatial distribution of the reaction-product species at the interface is governed by the competitive diffusion of N, Al, and B. Morphology of the reaction products are influenced by their orientation relationship with BNNT walls. A theoretical prediction on Al-BNNT interface in macroscale composite suggests the formation of strong bond between the matrix and reinforcement phase.

I. INTRODUCTION

Boron nitride nanotubes (BNNTs), the seamless cylindrical structures made of hexagonal boron nitride sheets possess excellent elastic modulus (~750–1200 GPa[1,2]) and strength (~61 GPa[3]). These unique properties of BNNTs have increased its potential as promising reinforcement to structural composites. BNNTs are relatively new in the field of composites with very few studies on them being available. BNNT-reinforced polymer composites have shown improvement in thermal, mechanical and optical properties.[4–9] Addition of BNNTs to aluminum oxide (Al_2O_3), silicon dioxide (SiO_2), trisilicon tetranitride (Si_3N_4), and hydroxyapatite ceramics have also resulted in improvement of elastic modulus, hardness, fracture toughness, flexural strength, and high-temperature superplasticity.[10–16] But, no report is available till date on metal matrix composites (MMCs), reinforced with BNNTs.

Aluminum-based MMCs are very attractive for structural applications due to light weight, good corrosion resistance, and high thermal and electrical conductivity. Carbon nanotubes (CNTs), which are structural analogue to BNNTs, are being researched for the past decade as a structural reinforcement to aluminum—primarily for the improvement of mechanical properties.[17–25] However, carbon nanotube-reinforced aluminum matrix (Al-CNT) composites have not resulted in the expected mechanical properties primarily due to CNT dispersion challenges and related weak matrix-reinforcement interface.[17,20,26] BNNT is a potential alternative to CNT for Al-matrix composites. Apart from having comparable elastic modulus and strength to CNTs, the structure of BNNT is more flexible

[a)]Address all correspondence to this author.
e-mail: agarwala@fiu.edu
DOI: 10.1557/jmr.2012.294

 © Materials Research Society 2012

https://doi.org/10.1557/jmr.2012.294 Published online by Cambridge University Press

and capable of withstanding heavy deformation without getting damaged.[27] BNNTs also possess higher fracture strain than CNTs.[28] Thus, it is of greater interest to evaluate the suitability of BNNTs as reinforcement in MMCs, including aluminum.

Matrix/reinforcement interface and interfacial reaction product are critical for the load-bearing capabilities in a composite material. In case of Al-CNT composites, aluminum carbide (Al_4C_3) formation at the interface has been addressed by several researchers.[18,26,29,30] It has been reported that a thick Al_4C_3 layer is deleterious to Al-CNT composite whereas thin (5–20 nm) layer promotes interfacial bonding.[17] Al_4C_3 formation is found even in rapid processing techniques, like plasma spraying and spark plasma sintering, which allows very short high-temperature exposure.[18,29] BNNT could be a better choice as the reinforcement as it possesses comparatively higher inertness than CNT.[27,31] BNNTs do not oxidize up to 950 °C, as compared with CNT, for which oxidation starts at 500 °C.[27,31] Also, the oxidation temperature for BNNT is much higher than melting point of aluminum (660 °C), which increases the feasibility of melt processing of Al-BNNT composite. Moreover, boron nitride coating on carbon fiber reinforcement is well accepted in ceramic matrix composites (CMCs) for enhancing the high-temperature strength and oxidation resistance.[32–34]

In the backdrop of this scenario, the objective of the present study was to understand reactions and their mechanisms occurring at Al-BNNT interface to establish the suitability of BNNT as a potential reinforcement for aluminum matrix. It is emphasized that there is no study in open literature that addresses the issues of Al-BNNT or any other metal-BNNT composite system. Understanding the nucleation and growth process of reaction products would give more control on the interface engineering, which is critical for the mechanical performance of any composite including Al-BNNT. A detailed high-resolution transmission electron microscopy (HRTEM) study on the size, morphology, and crystallographic orientation of the reaction products has been carried out to predict the stability of Al-BNNT interface in the composite structure. It must be noted that this study does not report on bulk-composite synthesis and mechanical characterization due to lack of availability of large amount of BNNTs.

II. MATERIALS AND METHODS

BNNTs, used in this study, were synthesized by a ball milling and annealing method. The details of the BNNT synthesis are presented in an earlier publication.[35] Figure 1(a) shows the scanning electron microscopy (SEM) image of the as-grown BNNTs. Transmission electron microscopy (TEM) observation of the BNNTs reveals their bamboo-shaped structure [Fig. 1(b)]. Bamboo-shaped BNNTs form due to slow nitriding reaction and enclosed metallic catalyst particles in BNNT tip.[36,37] Aluminum powder (≥99.7% Al) of spherical shape (H3, Valimet Inc.), with 90% particles (Stockton, CA) having diameter <10.5 μm, were used for preparing the composite powder.

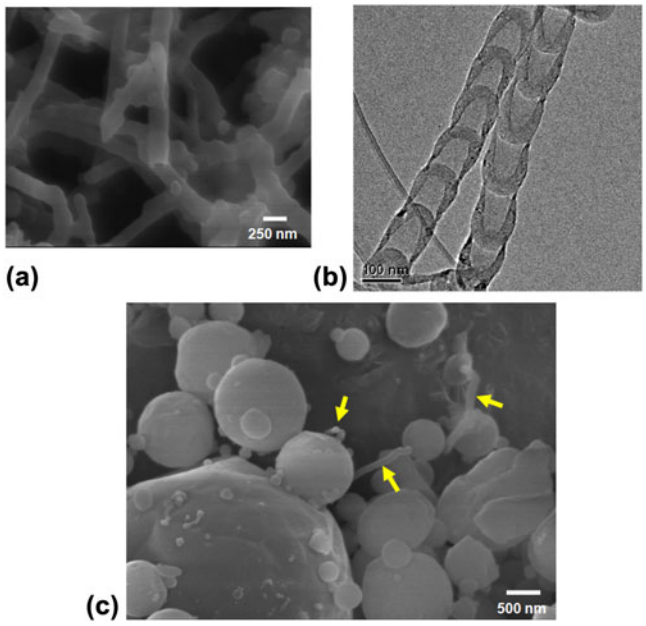


FIG. 1. (a) SEM and (b) TEM images of as-grown BNNTs; (c) SEM image Al-BNNT composite powder showing BNNTs dispersed in spherical Al powder particles.

Al-BNNT composite powder containing 5 vol% (4.23 wt%) reinforcement was prepared by wet-mixing method. The vol% of BNNT was calculated using BNNT density as 2.25 gm/cc. BNNTs were ultrasonicated in acetone for 1 h, followed by mixing of Al powder in the suspension and further ultrasonicating for 30 min. Drying of the composite powder was carried out in an oven at 60 °C for 2 h. Figure 1(c) shows the dispersed BNNTs in spherical Al powder particles after drying.

The composite powder was thermally treated at atmospheric pressure in argon (Ar) environment at 650 °C with a heating rate of 10 °C/min for soaking periods of 10, 60, and 120 min at peak temperature followed by furnace cooling in Ar. The composite powder was characterized for microstructure and chemical composition before and after thermal treatments to study the reactions occurring between BNNT and Al. X-ray diffraction (XRD) studies were carried out in a Siemens D-5000 x-ray diffractometer (Munich, Germany) using Cu K_α ($\lambda = 1.542$ Å) radiation. JEOL JSM-6330F field emission scanning electron microscope (FESEM; Tokyo, Japan) was used for the characterization of powders. TEM images of as-grown BNNTs and composite powders were captured using Philips/FEI Tecnai F30 HRTEM (Mahwah, NJ). Forward and inverse Fourier transform (FFT & Inverse-FFT) analysis, using Gatan, Inc. Digital Micrograph software, has been used for an accurate calculation of the lattice spacing.

https://doi.org/10.1557/jmr.2012.294 Published online by Cambridge University Press

III. RESULTS AND DISCUSSION

A. Thermodynamic prediction of reactions between Al and BNNT

The composite powder was heat-treated at 650 °C, a temperature close to the melting point of Al. The maximum soaking time was kept for 120 min. Such extreme processing conditions were chosen keeping in consideration the processing parameters that may be used for pressureless sintering or other consolidation methods to synthesize Al-BNNT composites. The idea was to evaluate the severe interfacial reactions that may occur during Al-BNNT composite fabrication. Thermodynamic feasibility of Al-BNNT reaction in experimental condition was evaluated using thermochemical software and database FactSage™.[38]

At 650 °C considering 5 vol% (4.23 g) BNNT addition in Al

$$(95.77)\mathrm{Al} + (4.23)\mathrm{BN} = (88.72)\mathrm{Al} + (6.98)\mathrm{AlN} + (4.14)\mathrm{AlB2}$$
$$\Delta G = -1.39 \times 10^4 \mathrm{J} \quad . \qquad (1)$$

The reaction shows formation of aluminum nitride (AlN) and aluminum diboride (AlB_2) at 650 °C with a negative change in Gibbs free energy (ΔG) indicating that reaction is thermodynamically feasible. But, this computation does not account for the kinetics of the reaction. Thus, it is not possible to estimate the extent of the reaction between Al and BNNT as a function of reaction time. However, the reactivity of Al with nitrogen (N) and boron (B) is evaluated separately to estimate the relative feasibility and mass of AlB_2 and AlN formation at the interface. Considering the alternating arrangement of B and N atoms in hexagonal rings on BNNT wall, breaking of bonds should release equal number of B and N atoms available for the reaction with Al.

At 650 °C considering 5 vol% BNNT addition in Al (the mass is in grams)

$$(95.77)\mathrm{Al} + (2.31)\mathrm{N_{gas}} = (91.69)\mathrm{Al} + (6.38)\mathrm{AlN}$$
$$\Delta G = -10.52 \times 10^4 \mathrm{J} \quad , \qquad (2)$$

$$(95.77)\mathrm{Al} + (1.83)\mathrm{B} = (93.48)\mathrm{Al} + (4.11)\mathrm{AlB2}$$
$$\Delta G = -0.51 \times 10^4 \mathrm{J} \quad . \qquad (3)$$

The comparison of Gibbs free energy values for the reactions (2) and (3) reveals formation of AlN to be thermodynamically more feasible than AlB_2. AlN also forms a larger mass fraction as compared with AlB_2. Similar density of AlN (3.26 g/cc) and AlB_2 (3.19 g/cc) ensures almost 1.55 times more volume for AlN than AlB_2. Thus, Factsage analysis of the possible interfacial reaction between BNNT and Al establishes the feasibility and relative amount of the reaction products.

B. Experimental validation of the reaction products at BNNT and Al interface

HRTEM was utilized to study the reaction products at BNNT and Al interface. Figure 2 shows BNNTs in the composite powder, exposed at 650 °C for different soaking periods, for a semiquantitative assessment of the extent of reaction-product generation as a function of time. Figure 2(a) shows the clean surface of as-grown BNNT (inset shows high magnification view). After 10 min of heat treatment, nucleation of discontinuous reaction product is observed at few locations [Fig. 2(b)]. The thickness of reaction layer is observed to increase further with time. A very thin, uneven and semicontinuous reaction layer is formed after 60 min of soaking [Fig. 2(c)]. Reaction-product volume increases from 60 to 120 min exposure resulting in much distinct globular crystals [Fig. 2(d)]. Reaction-product layer thickness is 0.35–2.3 nm (average: 1.5 nm) at 60 min and increases to 3.8–9 nm (average: 7.3 nm) at 120 min.

Figure 3 shows the XRD patterns for Al-BNNT composite powders at different heat-treated conditions. As mixed Al-BNNT powder shows only Al [Joint Committee on Powder Diffraction Standards (JCPDS) PDF: 01-071-3760]

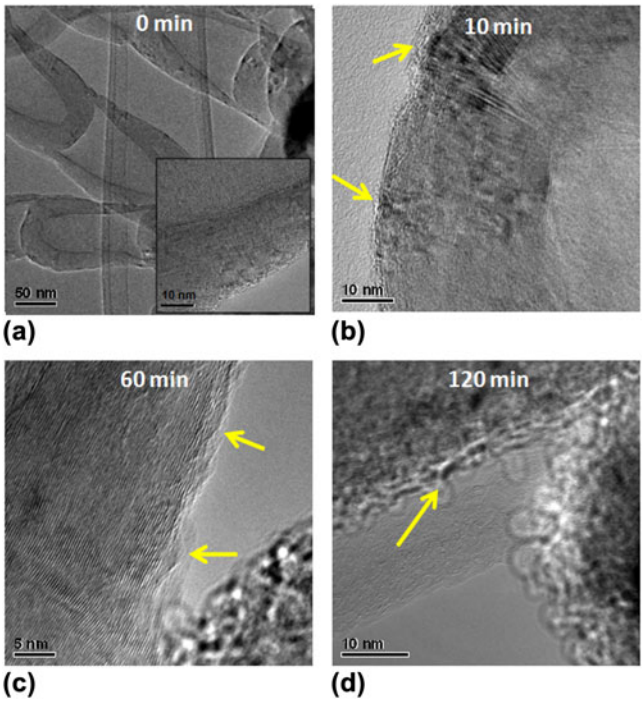


FIG. 2. High-resolution TEM images of BNNT in (a) as-grown condition; Al-BNNT composite powder heat-treated in argon at 650 °C for (b) 10 min, (c) 60 min, and (d) 120 min. Arrows indicate –reaction-product formation.

https://doi.org/10.1557/jmr.2012.294 Published online by Cambridge University Press

and very small hexagonal boron nitride (h-BN) (JCPDS PDF: 00-009–0012) peaks. Due to the low content in the composite powder, BNNTs generate very low peak intensity compared with Al. Thus the region of XRD patterns containing h-BN and other reaction-product peaks are magnified for their clear visualization and comparison. After 60 min exposure, the h-BN peak is still visible and comparable to its shape (sharpness) in untreated powder, which indicates negligible disorder in BNNT structure after 60 min of heat treatment. Very small and almost negligible peaks of AlB_2 (JCPDS PDF: 00-008-0216) in 60-min treated powder denotes minimal reaction-product formation. The presence of AlB_2 peak and absence of AlN in 60-min sample might seem to be not in perfect agreement with thermodynamic findings predicting more AlN formation than AlB_2. But, the XRD pattern is justifiable considering the relative crystal sizes of AlN and AlB_2, resulting from their differential nucleation and growth mechanism discussed in details in Sec. III. C. Small crystal size of AlN makes the peak very broad and diffused in background. On the contrary, a few AlB_2 crystals cause some constructive interference due to their larger size. After 120-min exposure, AlB_2 and AlN (JCPDS PDF: 00-003–1144) peaks start appearing with visible intensity, which confirms existence of these reaction products in reasonable amounts. The h-BN peak in this case is less sharp, which indicates more damage introduced in BNNT at 120 min of exposure. XRD pattern for the composite powder with 10-min heat treatment revealed peaks similar to untreated powder due to very short reaction time and hence is not plotted in Fig. 3.

The identity of the reaction products was further confirmed by determination of the lattice spacing in HRTEM image. Figure 4 presents the BNNT surface after heat treatment at 650 °C for 10 min, with trace of discretely nucleating crystals. The BNNTs surface at 10-min exposure was chosen for this observation because it is easier to identify single nucleating crystals at an early stage of the reaction. The population and size of these crystals will increase with heat-treatment duration, leading to more difficulty in identification via HRTEM. The measurement of the lattice spacing of the nucleating crystals reveals formation of AlN and AlB_2 phases. Figure 4 also reveals the crystallographic orientation relationship of these reaction products with BNNT wall, which is discussed in detail in Sec. III. C.

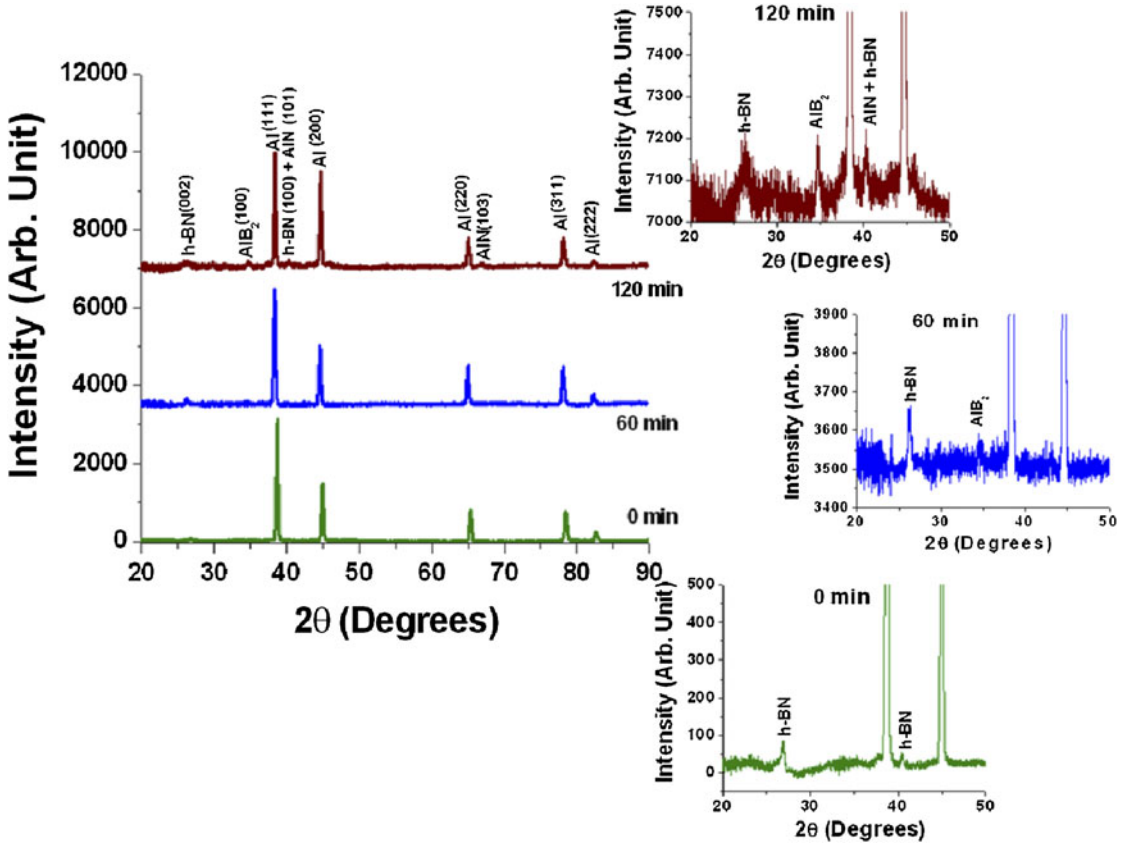


FIG. 3. XRD pattern of Al-BNNT composite powders in as-mixed condition (0 min) and heat-treated at 650 °C for 60 and 120 min. The pattern between 20–50° (2θ) is magnified for clear visualization of the small peaks resulting from BNNT and its reaction products AlN and AlB_2.

https://doi.org/10.1557/jmr.2012.294 Published online by Cambridge University Press

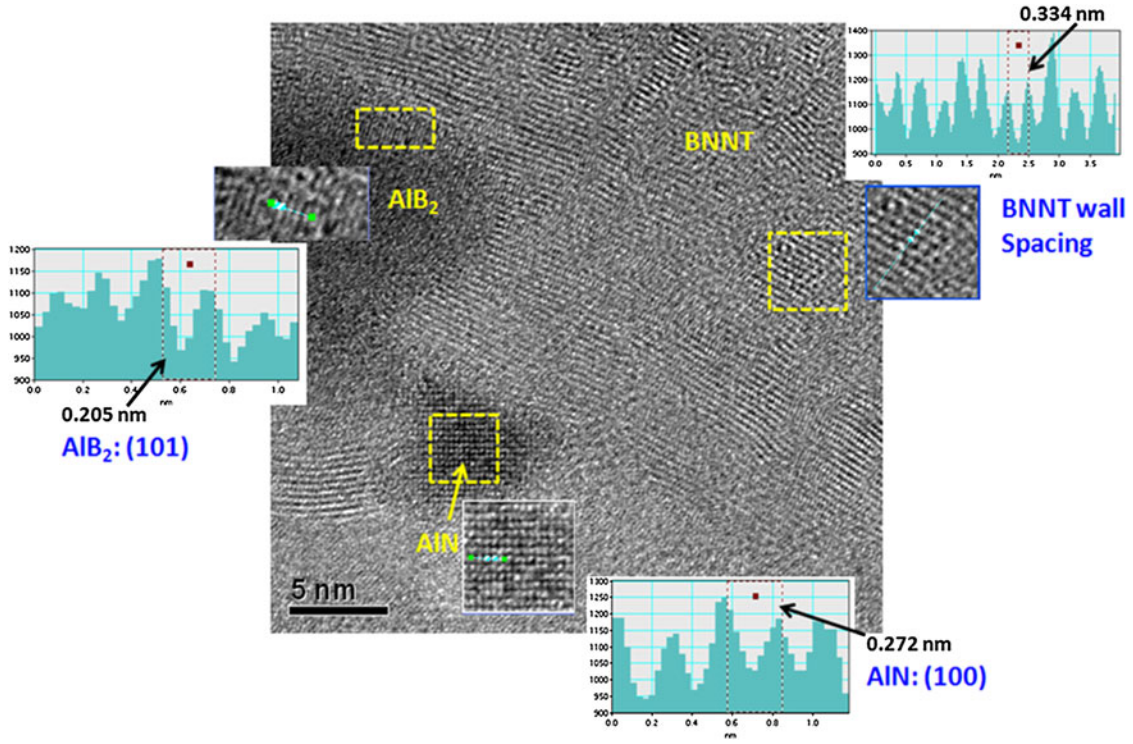


FIG. 4. Lattice image of Al-BNNT treated at 650 °C for 10 min reveals nucleation of AlN and AlB_2 crystals.

C. Reaction mechanisms

The nucleation and growth of reaction products depends on the competitive kinetics of the reactions among Al, B, and N. TEM images in Fig. 5 reveals the size and shape of AlN and AlB_2 crystals formed after 120 min of heat treatment of Al-BNNT powder. Figure 5(b) also reveals the presence of cobalt (II) nitrate [$Co(NO_3)_2$], which was used as the catalyst for BNNT growth and retained as impurity. AlN is observed as almost spherical crystals of ~7 nm size. On the contrary, AlB_2 develops into an elongated and big crystal with ~35 nm length, which is five times larger than AlN. The size, shape and spatial distribution of the reaction products are attributed to: (i) growth mechanism of AlN and AlB_2 and their orientation with BNNT wall, and (ii) diffusion of Al, B, and N in each other through interface of Al and BNNT.

The crystallographic orientation relation of AlN and AlB_2 with BNNT surface could best be observed at nucleation or early stage of growth. Thus, the 10-min heat-treated composite powder was chosen for this analysis. Figure 6 presents the same micrograph as Fig. 4 but with additional orientation relationships. Figure 4 was not used for this purpose as too many markings would obstruct the proper visualization of the HRTEM micrograph. The (100) planes of AlN is found to make 23° angle with BNNT wall (Fig. 6). This indicates that the c-axis of hexagonal wurtzite-type crystals of AlN[39] will be aligned at 23° to BNNTs walls. AlN crystals are reported to have a favorable growth direction along c-axis.[40–42] Thus several crystals of AlN nucleated on BNNT surface would hinder the growth of each other due to their low angle (23°) alignment with BNNT wall along growth direction (c-axis). This competition between growing crystals results in smaller size of AlN crystals (~7 nm) at Al-BNNT interface. On the other hand, AlB_2 crystals nucleate with (101) set of planes at 90° to the BNNT surface (Fig. 6). Considering the hexagonal structure of AlB_2 with alternate arrangement of hexagonal layers of Al and B,[43] the basal plane of this crystal makes 38.6° angles with BNNT wall. The AlB_2 crystals prefer to grow along their basal plane, similar to graphite structure, forming plate-like morphology.[44] In case of AlB_2, comparatively higher angular alignment of growth direction with BNNT surface (38.6°) allows its growth to larger sizes. In addition, the natural tendency of AlB_2 for growing into large crystals at the expense of smaller crystals[44] helps in formation of crystals approximately five times larger than AlN. Figure 5(b) reveals the elongated direction of AlB_2 particles to be approximately at 58° to (101) planes. The angular difference between basal and (101) set of planes in AlB_2 is also in similar range (51.4°), confirming basal planar growth of AlB_2, as observed in other studies.[44]

The spatial distribution of AlN and AlB_2 across the interface also depends on the relative diffusivity of Al, B, and N in each other. Smaller N atoms [atomic radius: 65 picometer (pm)] diffuse faster in Al than B (atomic

https://doi.org/10.1557/jmr.2012.294 Published online by Cambridge University Press

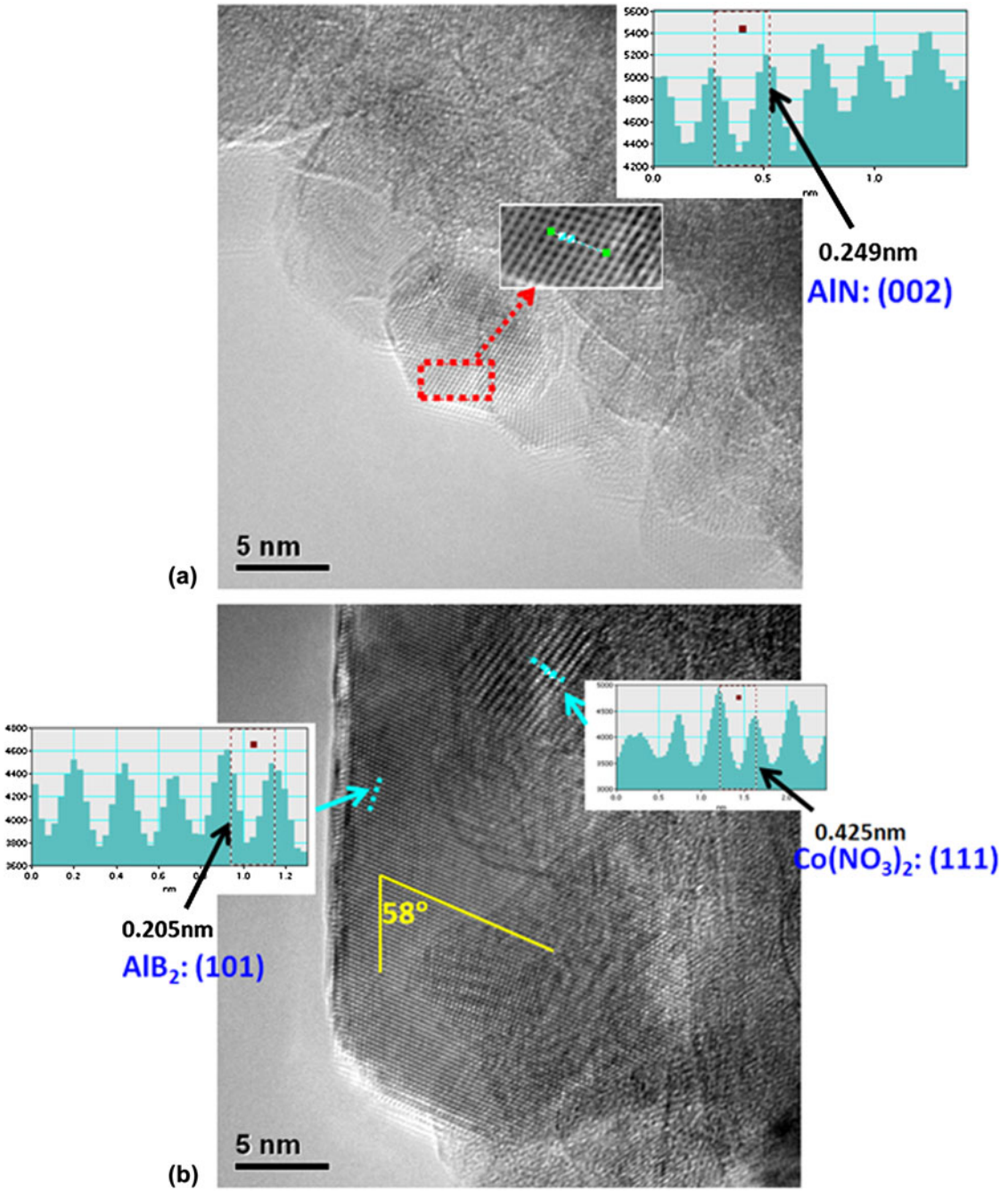


FIG. 5. Reaction-product growth on BNNT surface for 120-min treated powder—revealing morphology and shape of (a) AlN and (b) AlB_2 crystals. Cobalt (Co)-nitrate [$Co(NO_3)_2$] was used as catalyst for BNNT growth—some impurities of unreacted Co-nitrate are also observed on BNNT surface.

radius: 85 pm), leading to more AlN formation toward Al side of the interface. Thus a higher concentration of B atoms is created toward BN side of the interface. Previous studies on Al-BN system have confirmed the formation of AlN ahead of AlB_2 through differential scanning calorimetric analysis.[45] Xue et al. have also observed similar phenomenon occurring at Al-hBN interface, followed by the penetration of molten Al through BN ceramic surface.[46] The heat-treatment temperature (650 °C) used in the present study is slightly lower than melting point of Al and thus melting of Al is not expected. But, at this high temperature Al is highly thermally active and diffuses fast through BN surface to form AlB_2. A closer observation of Fig. 6 confirms nucleation of AlN on the outer surface of BNNT. Similarly, left behind B atoms react with inwardly diffusing Al atoms to nucleate AlB_2 at grooves in surfaces of BNNT wall.

https://doi.org/10.1557/jmr.2012.294 Published online by Cambridge University Press

The extent of reaction on Al-BNNT interface is also influenced by morphological features and defects in BNNT surface and structure. Reaction is found to occur largely on the outer wall of BNNT with clean inner walls even after 120-min high-temperature exposure [Fig. 7(a)].

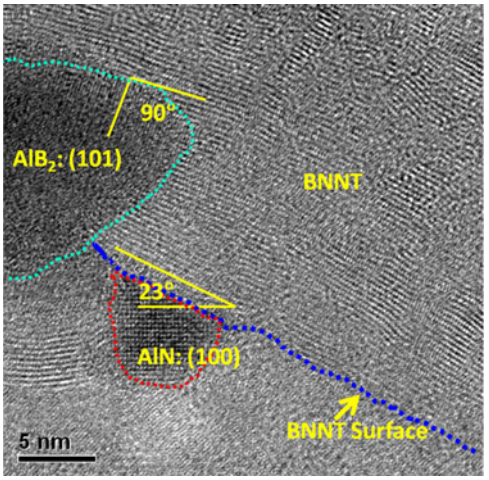


FIG. 6. Orientation relationship of AlN and AlB_2 crystals grown on BNNT surface treated at 650 °C for 10 min. The BNNT is outlined in blue. AlN crystal on surface of BNNT is marked in red and AlB_2 in the groove of BNNT surface with cyan.

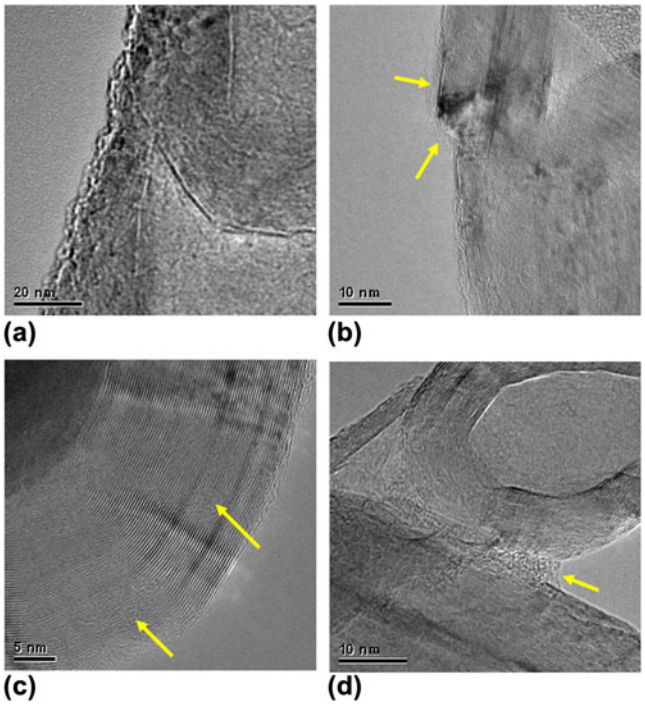


FIG. 7. (a) Reaction-product formation at the outer wall of BNNT surface after 120 min of treatment. Inner walls are intact. (b) Reaction in the vicinity of broken wall of BNNT after 10 min of treatment; (c) thermal disturbance at knot/joint of bamboo-shaped BNNT after 10 min of treatment; (d) preferential reaction-product formation at knot/joint of BNNT after 60 min of heat treatment.

This observation indicates that the reaction starts at the outer wall of BNNT and would take significantly long time for destroying the entire BNNT structure. The intact bamboo-shaped structure of BNNT without structural damage is clearly observed in Fig. 7(a). The damaged or broken sites on the surface of BNNT are more prone to reaction-product formation. Figure 7(b) shows visible/significant amount of reaction-product formation at the broken wall of BNNT after mere 10 min of heat treatment, whereas minimum or negligible reaction product is noticeable on the defect-free surface with the same treatment [Fig. 2(b)]. This is attributed to accelerated diffusion kinetics caused by defects in BNNT wall. Defects on BNNT walls can also be created by thermal disturbance introduced in the lattice structure, when exposed at high temperature. The area that is more prone to such thermal disturbance is the knots of the bamboo-shaped BNNTs. The knot/joint regions of bamboo-shaped BNNTs form an interlocked type of structure and experience compressive interfacial stresses.[47] Preexisting stresses in the joint regions cause disturbances to the structure under thermal exposure easily. An evidence of patches of thermally disturbed region is observed in the joint region of BNNT in Fig. 7(c). Disturbance of the lattice structure throughout the thickness of BNNT wall, at 10-min thermal exposure is attributed to the additional energy available from structural compressive stress present in knots. If the BNNT is broken and the surface of the knot is exposed, then more reaction can take place in that region. In addition, the unstable dangling bonds at joints of bamboo-shaped BNNTs are found leading to highly reactive properties.[36]

Figure 7(d) presents evidence of preferential reaction-product formation at exposed BNNT joint after 60-min

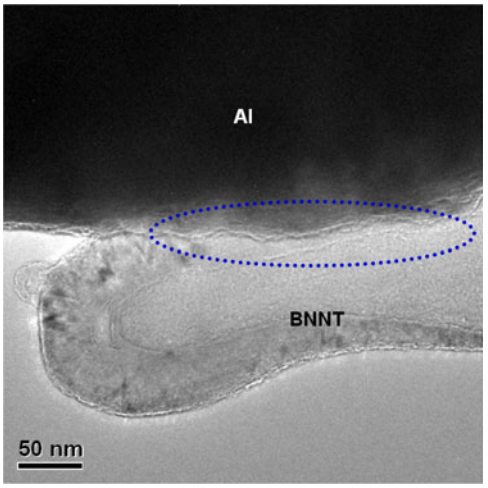


FIG. 8. A broken piece of BNNT in Al-BNNT composite powder—exposed for 60 min at 650 °C. The upper part of BNNT wall (marked) is mostly consumed by severe reaction with adjacent Al particle.

https://doi.org/10.1557/jmr.2012.294 Published online by Cambridge University Press

thermal exposure. Broken BNNT pieces are also more prone to reaction due to exposure of more surface area, which increases diffusion. Figure 8 presents the HRTEM images of a one-knot length broken BNNT piece severely damaged and reacted throughout its wall thickness at 60-min thermal exposure. The marked portion of the image shows that the wall of BNNT is significantly thinned down due to severe reaction with adjacent Al particle. Hence, it is important to have unbroken and long BNNTs as reinforcement in metal matrix composites.

D. Prediction of Al-BNNT interface in macroscale composite

The reaction at Al-BNNT interface has been dealt at submicrometer level till now. The aim of this section is to predict the behavior of Al-BNNT interface in the macroscale composite structure, which is critical for improved mechanical properties. The nature of Al-BNNT interface will be governed by the following major factors: (i) thickness of the reaction-product layer at the interface; and (ii) phase coherency of the reaction products along interface.

Thickness of the reaction product is significant for the Al/BNNT interface on two counts. First, thick reaction-product layer formed at the expense of the reinforcement would make the BNNT weak rendering it unsuitable for performing its function in the structural composite. Second, very thick (>100 nm) reaction product at the interface could cause poor bonding of BNNT reinforcement to Al matrix and serve as a weak point for the mechanical failure. In our study, BNNTs are found retaining its bamboo-shaped cylindrical structure [Fig. 9(a)] surviving severe thermal conditions, which is near the melting point of Al. Exposure of the composite powder at 650 °C for 120 min ensures that BNNTs can withstand near-melting fabrication environment for Al-based composites. The average thickness of the reaction products formed between Al and BNNT interface is very thin (1.5 nm for 60-min treatment). In addition, reaction products form a bond between Al and BNNT at interface [Fig. 9(b)], which helps in integration of the reinforcement in the matrix. The thickness of the reaction product in Al-BNNT is compared with that of Al-CNT system, as the latter is well studied and analogous to BNNT. Aluminum carbide (Al_4C_3) layer formation in large amount at matrix-reinforcement (Al-CNT) interface is found deleterious to mechanical performance of the composite, due to inherent brittleness and hygroscopic nature of the carbide.[17,20,48–50] In comparison, the reaction products (AlB_2 and AlN) in Al-BNNT system are not so detrimental as Al_4C_3. AlN reinforcement improves the hardness and flexural strength of Al-based composites.[51,52] AlB_2 is also least detrimental to the fracture toughness of Al-based composite as compared with Al_4C_3, when formed simultaneously in a composite interface.[53,54] Thus, a small amount

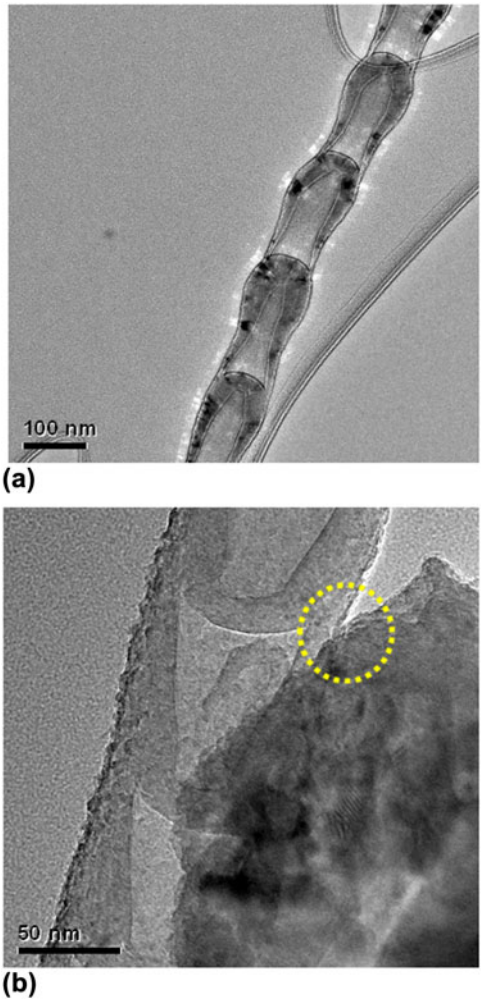


FIG. 9. (a) Retention of bamboo-shaped BNNT structure in Al-BNNT powder treated at 650 °C for 120 min; (b) bonding at Al/BNNT interface through the reaction product due to heat treatment at 650 °C for 120 min.

of nitride and boride formation in Al-based composites is not as deleterious as compared with carbides. Even so, it is always preferable to have a thin interfacial layer, as higher content of reaction-product formation thins down and shortens the fiber-shaped reinforcement making it less effective in load bearing, which is undesirable. Thermodynamic analysis on the probability of reaction between Al and C using Factsage™ is represented as:

At 650 °C considering 4.23 g of C addition in Al

$$(95.77)\mathrm{Al} + (4.23)\mathrm{C} = (83.10)\mathrm{Al} + (16.9)\mathrm{Al_4C_3}$$
$$\Delta G = -2.07 \times 10^4\ \mathrm{J} \quad . \qquad (4)$$

Comparison between Eqs. (1) and (4) reveals ΔG with higher negative value for Al-CNT system, which indicates higher feasibility of carbide formation at 650 °C. The amount of reaction product in case of CNT is also ~1.5 times more per unit mass of the product as compared with BNNT. In

https://doi.org/10.1557/jmr.2012.294 Published online by Cambridge University Press

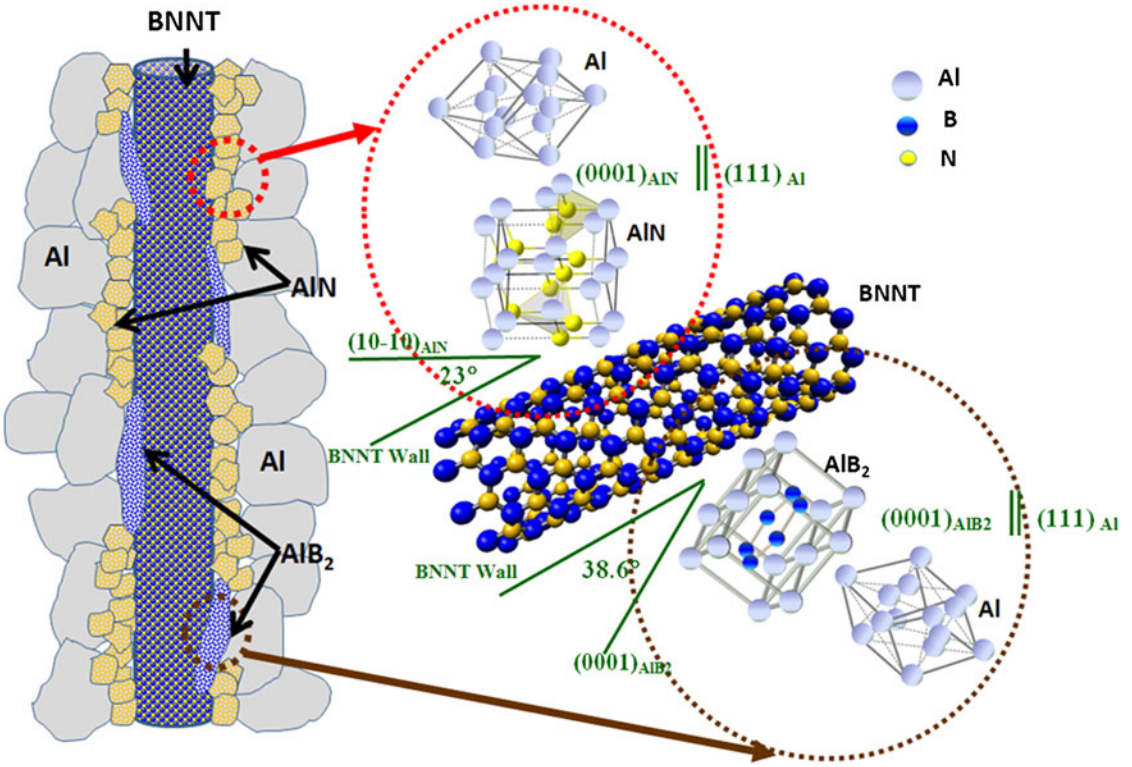


FIG. 10. Schematic of Al-BNNT interface revealing spatial distribution of reaction products across the interface and the crystallographic orientation of the products with BNNT on one side and Al on the other.

addition to the thermodynamic feasibility, a kinetic feasibility of reactions can be assessed by comparing of the results from the present study with the reports available of Al-CNT system.[18,29,30] Spark plasma sintering of Al-CNT at 600 °C for 20-min results in 20- to 40-nm thick carbide formation at Al-CNT interface.[18] Compared with these results, the reaction-product formation rate is much lower in Al-BNNT interface. Thermal exposure for 60 min at 650 °C causes mere 1.5-nm thick reaction-product formation, whereas 120-min exposure causes approximately 7-nm thick layer at interface. Thin layer of interfacial product is found promoting the interfacial locking of the reinforced nanotubes in Al matrix.[18,30] Thus, thin reaction-product layer at Al-BNNT interface should result in better locking of BNNTs in Al matrix. In addition, the closed end of the bamboo-shaped BNNT would cause reaction-product formation at tip also, resulting in pinning of the nanotube to the matrix.[18,30]

The interfacial orientation relationship between the reaction product and Al matrix is also important for determining the interfacial strength of the composite. AlN is reported to form a stable interface[55] along Al (111) and AlN (002) crystallographic orientation. Al (111) and AlN (002) surfaces form the lowest energy coherent interface[56] and helps in bonding of reinforcement with matrix. AlN crystals are more equiaxed, which denotes coherency of second phase in the matrix with less misfit strain. On the contrary, interfacial energy of Al/AlB_2 interface is much higher than that between Al grains,[57] as they have only one set of partially coherent planes between Al and AlB_2.[58] This makes the Al-AlB_2 interface weaker than Al-AlN. In addition, shape of AlB_2 is elongated, which means a semi-coherent boundary of the second phase with the matrix. But the larger edge of AlB_2 shows less misfit strain than the thinner edge (thickness). Hence, most part of AlB_2 phase would also offer better bonding with the matrix. It has been observed earlier that AlN crystals will mostly cover the surface of BNNTs with embedded AlB_2 at few locations. Since A1N forms a more stable interface, it is expected to result in a strong interfacial bonding between A1 and BNNT. Few locations having Al-AlB_2 interface might show a weaker bonding. However, more spatial coverage of Al-AlN along-with its stable coherent bonding nature would provide a strong interface between BNNT reinforcement and Al matrix in the composite structure.

Figure 10 presents a schematic of Al-BNNT interface with spatial distribution of reaction products and their orientation relationship with BNNT on one side and Al on other. This schematic helps in visualization and understanding of the interface in Al-BNNT composite structure. AlN covers more area on BNNT surface. Thus, Al-BNNT interface would show good adhesion due to the enhancing effect of stable Al-AlN interface, which is more prevalent than weaker Al-AlB_2 interface. The findings of

https://doi.org/10.1557/jmr.2012.294 Published online by Cambridge University Press

this investigation demonstrate the feasibility of fabrication of bulk Al-BNNT composite, which is being pursued by our research groups through large-scale synthesis of BNNTs and spark plasma sintering/hot pressing consolidation respectively.

IV. SUMMARY

This study deals with the mechanism of reaction-product formation at Al-BNNT interface during thermal exposure. Reaction-product formation rate is very slow at Al-BNNT interface with only 1.5-nm thick layer formed at 60-min exposure and 7 nm at 120 min near the melting point of aluminum (650 °C). Both AlN (Wurtzite) and AlB_2 (layered hexagonal) are found forming at the interface with different nucleation and growth mechanism. Faster outward diffusion of N from BN in Al leads to nucleation of AlN crystals at the outer surface of BNNT toward Al side. On the other hand, thermally activated Al atoms diffuse to the leftover B-concentrated regions to form AlB_2 in the grooves of BNNT wall. AlN forms numerous small and equiaxed crystals, whereas AlB_2 grows into large and elongated grains. Broken wall or joints of bamboo region of BNNT also influences the localized rate of reaction. A comparison of Al-BNNT with the analogous Al-CNT system reveals more feasibility and amount of reaction-product formation in case of latter, which could be deleterious to the structural integrity. Al-BNNT interface in the macroscale composite structure is expected to have a strong matrix-reinforcement bonding due to the stable orientation relationship between Al and AlN crystals that covers major part of the interface. It is proposed that BNNT could serve as an effective reinforcement for aluminum matrix composites.

ACKNOWLEDGMENTS

A.A. would like to acknowledge support from National Science Foundation CAREER Award (NSF-DMI-0547178) and U.S. Air Force Office of Scientific Research through FA9550-09-1-0297 and DURIP (FA9550-11-1-0334) grants. The overall support of Mr. Neal Ricks and AMERI at FIU, in maintaining the research facilities are greatly acknowledged.

REFERENCES

1. A.P. Suryavanshi, M.F. Yu, J. Wen, C. Tang, and Y. Bando: Elastic modulus and resonance behavior of boron nitride nanotubes. *Appl. Phys. Lett.* **84**, 2527 (2004).
2. N.G. Chopra and A. Zetll: Measurement of the elastic modulus of a multiwalled boron nitride nanotubes. *Solid State Commun.* **105**, 297 (1998).
3. R. Arenal, M-S. Wang, Z. Xu, A. Loiseau, and D. Golberg: Young modulus, mechanical and electrical properties of isolated individual and bundled single-walled boron nitride nanotubes. *Nanotechnology* **22**, 265704 (2011).
4. C. Zhi, Y. Bando, C. Tang, S. Honda, K. Sato, H. Kuwahara, and D. Golberg: Characteristics of boron nitride nanotube–polyaniline composites. *Angew. Chem.* **44**, 7929 (2005).
5. C. Zhi, Y. Bando, and C. Tang: Boron nitride nanotube/polystyrene composites. *J. Mater. Res.* **21**, 2794 (2006).
6. C. Zhi, Y. Bando, T. Terao, C. Tang, H. Kuwahara, and D. Golberg: Towards thermoconductive, electrically insulating polymeric composites with boron nitride nanotubes as fillers. *Adv. Funct. Mater.* **19**, 1857 (2009).
7. T. Terao, C. Zhi, Y. Bando, M. Mitome, C. Tang, and D. Golberg: Alignment of boron nitride nanotubes in polymeric composite films for thermal conductivity improvement. *J. Phys. Chem.* **114**, 4340 (2010).
8. J. Ravichandran, A.G. Manoj, J. Liu, I. Manna, and D.L. Carroll: A novel polymer nanotube composite for photovoltaic packaging applications. *Nanotechnology* **19**, 085712 (2008).
9. D. Lahiri, F. Rouzaud, T. Richard, A.K. Keshri, S.R. Bakshi, L. Kos, and A. Agarwal: Boron nitride nanotube-reinforced polylactide–polycaprolactone copolymer composite: Mechanical properties and cytocompatibility with osteoblasts and macrophages in vitro. *Acta Biomater.* **6**, 3524 (2010).
10. Q. Huang, Y. Bando, X. Xu, T. Nishimura, C. Zhang, C. Tang, F. Xu, L. Gao, and D. Golberg: Enhancing superplasticity of engineering ceramics by introducing BN nanotubes. *Nanotechnology* **18**, 485706 (2007).
11. D. Lahiri, V. Singh, A.P. Benaduce, S. Seal, L. Kos, and A. Agarwal: Boron nitride nanotube-reinforced hydroxyapatite composite: Mechanical and tribological performance and in vitro biocompatibility to osteoblasts. *J. Mech. Behav. Biomed. Mater.* **4**, 44 (2011).
12. M. Du, J-Q. Bi, W-L. Eang, X-L. Sun, and N-N. Long: Microstructure and properties of SiO_2 matrix reinforced by BN nanotubes and nanoparticles. *J. Alloys Compd.* **509**, 9996 (2011).
13. W-L. Wang, J-Q. Bi, K-N. Sun, M. Du, N-N. Long, and Y-J. Bai: Fabrication of alumina ceramic reinforced with boron nitride nanotubes with improved mechanical properties. *J. Am. Ceram. Soc.* **94**, 3636 (2011).
14. W-L. Wang, J-Q. Bi, K-N. Sun, M. Du, N-N. Long, and Y-J. Bai: Thermal shock resistance behavior of alumina ceramics incorporated with boron nitride nanotubes. *J. Am. Ceram. Soc.* **94**, 2304 (2011).
15. W-L. Wang, J-Q. Bi, S-R. Wang, K-N. Sun, M. Du, N-N. Long, and Y-J. Bai: Microstructure and mechanical properties of alumina ceramics reinforced by boron nitride nanotubes. *J. Eur. Ceram. Soc.* **31**, 2277 (2011).
16. M. Du, J-Q. Bi, W-L. Wang, X-L. Sun, N-N. Long, and Y-J. Bai: Fabrication and mechanical properties of SiO_2–Al_2O_3–BNNPs and SiO_2–Al_2O_3–BNNTs composites. *Mater. Sci. Eng., A* **530**, 669 (2011).
17. A. Agarwal, S.R. Bakshi, and D. Lahiri: *Carbon Nanotubes: Reinforced Metal Matrix Composites* (CRC Press, Boca Raton, FL, 2010), ISBN: 9781439811498.
18. H. Kwon, M. Estili, K. Takagi, T. Miyazaki, and A. Kawasaki: Combination of hot extrusion and spark plasma sintering for producing carbon nanotube reinforced aluminum matrix composites. *Carbon* **47**, 570 (2009).
19. T. Laha, A. Agarwal, T. McKechnie, and S. Seal: Synthesis and characterization of plasma spray-formed carbon nanotube-reinforced aluminum composite. *Mater. Sci. Eng., A* **381**, 249 (2004).
20. S.R. Bakshi, D. Lahiri, and A. Agarwal: Carbon nanotube reinforced metal matrix composites—A review. *Int. Mater. Rev.* **55**, 41 (2010).
21. T. Laha, S. Kuchibatla, S. Seal, W. Li, and A. Agarwal: Interfacial phenomena in thermally sprayed multiwalled carbon nanotube reinforced aluminum nanocomposite. *Acta Mater.* **55**, 1059 (2007).
22. C.F. Deng, D.Z. Wang, X.X. Zhang, and A.B. Li: Processing and properties of carbon nanotubes-reinforced aluminum composites. *Mater. Sci. Eng., A* **444**, 138 (2007).

https://doi.org/10.1557/jmr.2012.294 Published online by Cambridge University Press

23. C. He, N. Zhao, C. Shi, X. Du, J. Li, H. Li, and Q. Cui: An approach to obtaining homogeneously dispersed carbon nanotubes in Al powders for preparing reinforced Al-matrix composites. *Adv. Mater.* **19**, 1128 (2007).
24. H. Choi, J. Shin, B. Min, J. Park, and D. Bae: Reinforcing effects of carbon nanotubes in structural aluminum matrix nanocomposites. *J. Mater. Res.* **24**, 2610 (2009).
25. R. Pérez-Bustamante, C.D. Gómez-Esparza, I. Estrada-Guel, M. Miki-Yoshida, L. Licea-Jiménez, S.A. Pérez-García, and R. Martínez-Sánchez: Microstructural and mechanical characterization of Al–MWCNT composites produced by mechanical milling. *Mater. Sci. Eng., A* **502**, 159 (2009).
26. S.R. Bakshi and A. Agarwal: An analysis on the factors affecting strengthening in carbon nanotube-reinforced aluminum composites. *Carbon* **49**, 533 (2011).
27. D. Golberg, Y. Bando, C. Tang, and C. Zhi: Boron nitride nanotubes. *Adv. Mater.* **19**, 2413 (2007).
28. H.M. Ghassemi, C.H. Lee, Y.K. Yap, and R.S. Yassar: In situ observation of reversible rippling in multiwalled boron nitride nanotubes. *Nanotechnology* **22**, 115702 (2011).
29. S.R. Bakshi, A.K. Keshri, V. Singh, S. Seal, and A. Agarwal: Interface in carbon nanotube-reinforced aluminum silicon composites: Thermodynamic analysis and experimental verification. *J. Alloys Compd.* **48**, 207 (2009).
30. L. Ci, Z. Ryu, N.Y. Jin-Phillipp, and M. Ruhle: Investigation of the interfacial reaction between multiwalled carbon nanotubes and aluminum. *Acta Mater.* **54**, 5367 (2006).
31. D. Golberg, Y. Bando, K. Kurashima, and T. Sato: Synthesis and characterization of ropes made of BN multiwalled nanotubes. *Scr. Mater.* **44**, 1561 (2001).
32. M. Das, J. Ghosh, and A.K. Basu: Effect of activation on boron nitride coating on carbon fiber. *Ceram. Int.* **36**, 2511 (2010).
33. M. Das, A.K. Basu, S. Ghatak, and A.G. Joshi: Carbothermal synthesis of boron nitride coating on PAN carbon fiber. *J. Eur. Ceram. Soc.* **29**, 2129 (2009).
34. E. Pippel, J. Woltersdorf, D. Dietrich, S. Stockel, K. Weise, and G.J. Marx: CVD-coated boron nitride on continuous silicon carbide fibers: Structure and nanocomposition. *J. Eur. Ceram. Soc.* **20**, 1837 (2000).
35. L.H. Li, Y. Chen, and A.M. Glishenkov: Synthesis of boron nitride nanotubes by boron ink annealing. *Nanotechnology* **21**, 105601 (2010).
36. C-Y. Su, Z-Y. Juang, K-F. Chen, B-M. Cheng, F-R. Chen, K-C. Leou, and C-H. Tsai: Selective growth of boron nitride nanotubes by the plasma-assisted and iron-catalytic CVD methods. *J. Phys. Chem.* **113**, 14681 (2009).
37. J. Yu, B.C.P. Li, J. Zou, and Y. Chen: Influence of nitriding gases on the growth of boron nitride nanotubes. *J. Mater. Sci.* **42**, 4025 (2007).
38. C.W. Bale, P. Chartrand, S.A. Degterov, G. Eriksson, K. Hack, R. Ben Mahfoud, J. Melançon, A.D. Pelton, and S. Petersen: FactSage thermochemical software and databases. *CALPHAD* **26**, 189 (2002).
39. Y. Taniyasu and M. Kasu: Improved emission efficiency of 210-nm deep ultraviolet aluminum nitride. *NTT Tech. Rev.* **8**, 1 (2010).
40. H. Lv, G. Chen, H. Ye, and G. Yan: Synthesis of monocrystal aluminum nitride nanowires at low temperature. *J. Appl. Phys.* **101**, 053526 (2007).
41. J. Yang, T-W. Liu, C-W. Hsu, L-C. Chen, K-H. Chen, and C-C. Chen: Controlled growth of aluminum nitride nanorod arrays via chemical vapor deposition. *Nanotechnology* **17**, S321 (2006).
42. F. Martin, P. Muralt, M-A. Dubois, and A. Pezous: Thickness dependence of the properties of highly c-axis textured AlN thin films. *J. Vac. Sci. Technol., A* **22**, 361 (2004).
43. D. Larbalesiter, A. Gurevich, D.M. Feldmann, and A. Polyanskii: High-Tc superconducting materials for electric power applications. *Nature* **414**, 368 (2001).
44. C. Deppisch, G. Liu, A. Hall, Y. Xu, A. Zangvil, J.K. Shang, and J. Economy: The crystallization and growth of AlB_2 single crystal flakes in aluminum. *J. Mater. Res.* **13**, 3485 (1998).
45. C. Du, S. Li, K. Zhang, and K. Lu: BN/Al composite formation by high energy ball milling. *Scr. Mater.* **36**, 7 (1997).
46. X.M. Xue, J.T. Wang, and M.X. Quan: Wetting characteristics and interfacial reaction of liquid aluminum on hot-pressed boronde substrate. *Mater. Sci. Eng., A* **132**, 277 (1991).
47. D-M. Tang, C-L. Ren, X. Wei, M-S. Wang, C. Liu, Y. Bando, and D. Golberg: Mechanical properties of bamboo-like boron nitride nanotubes by in-situ TEM and MD simulations: Strengthening effect of interlocked joint interfaces. *ACS Nano* **5**, 7362 (2011).
48. S.R. Bakshi, A.K. Keshri, and A. Agarwal: A comparison of mechanical and wear properties of plasma sprayed carbon nanotube reinforced aluminum composites at nano- and macroscale. *Mater. Sci. Eng., A* **528**, 3375 (2011).
49. I-Y. Kim, J-H. Lee, G-S. Lee, S-H. Baik, Y-J. Kim, and Y-Z. Lee: Friction and wear characteristics of the carbon nanotube–aluminum composites with different manufacturing conditions. *Wear* **267**, 593 (2009).
50. T. Etter, P. Schulz, M. Weber, J. Metz, M. Wimmler, J.F. Loffler, and P.J. Uggowitzer: TEM observation of liquid-phase bonded aluminum–silicon/aluminum nitride hetero interface. *Mater. Sci. Eng., A* **448**, 1 (2007).
51. M. Naranjo, J.A. Rodriguez, and E.J. Herrera: Sintering of Al/AlN composite powder obtained by gas–solid reaction milling. *Scr. Mater.* **49**, 65 (2003).
52. D-F. Lii, J-L. Huang, and S-T. Chang: The mechanical properties of AlN/Al composites manufactured by squeeze casting. *J. Eur. Ceram. Soc.* **22**, 253 (2002).
53. B-S. Lee and S. Kang: Low-temperature processing of B_4C–Al composites via infiltration technique. *Mater. Chem. Phys.* **67**, 249 (2001).
54. G. Arslan, F. Kara, and S. Turan: Quantitative x-ray diffraction analysis of reactive infiltrated boron carbide–aluminum composites. *J. Eur. Ceram. Soc.* **23**, 1243 (2003).
55. C.M. Montesa, N. Shibata, T. Tohei, and Y. Ikuhara: TEM observation of liquid-phase bonded aluminum–silicon/aluminum nitride hetero interface. *J. Mater. Sci.* **46**, 4392 (2011).
56. X.L. Xiao, D.G. McCulloch, D.R. Mckenzie, and M.M.M. Bilek: The microstructure and stability of Al/AlN multilayered films. *J. Appl. Phys.* **100**, 013504 (2006).
57. Y.F. Han, Y.B. Dai, J. Wang, D. Shu, and B.D. Sun: First-principles calculations on Al/AlB_2 interfaces. *Appl. Surf. Sci.* **257**, 7831 (2011).
58. H-H. Zhang: Crystallography and refining mechanism of (Ti, B)-contained salts in pure aluminum. *Trans. Nonferrous Met. Soc. China* **18**, 836 (2008).

https://doi.org/10.1557/jmr.2012.294 Published online by Cambridge University Press